PCCP

PAPER

View Article Online
View Journal | View Issue

Cite this: *Phys. Chem. Chem. Phys.*, 2014, **16**, 6294

Photodissociation dynamics of propargylene, HCCCH†

Jens Giegerich, Jens Petersen, Roland Mitrić* and Ingo Fischer*

Received 30th July 2013,
Accepted 6th February 2014

DOI: 10.1039/c3cp53213e

www.rsc.org/pccp

We report a joint theoretical and experimental study on the photodissociation of the C_3H_2 isomer propargylene, HCCCH, combining velocity map imaging with nonadiabatic trajectory surface hopping calculations. Propargylene loses an H-atom, after laser excitation at around 250 nm, presumably to the T_6 state. The photofragment angular distribution exhibits only a very small anisotropy, but the H-atom translational energy distribution extends to high energies and shows an expectation value of $\langle f_T \rangle$, the fraction of excess energy released as translation, of 48%, outside the range expected for a statistical reaction mechanism. The computations suggest a predissociation in the T_4–T_6 state and lead to a translational energy distribution and photofragment angular distribution that match the experimentally observed ones very well.

A Introduction

The three isomers of the carbene C_3H_2 are important intermediates in reactive environments. Cyclopropenylidene, c-C_3H_2, is one of the most abundant organic molecules in interstellar clouds[1–3] and propadienylidene, H_2CCC, has been suggested as a carrier of the diffuse interstellar bands (DIB).[4,5] The third isomer is propargylene, HCCCH, depicted in the centre of Fig. 1, also called propynylidene. It has not yet been detected in space due to its small dipole moment, but it has been found in fuel-rich flames[6] and is considered to be a soot precursor. All three molecules are of interest to theory, because they possess low-lying electronically excited states that are subject to vibronic coupling. While H_2CCC has been studied extensively,[7,8] only limited data are available for HCCCH. It has a triplet ground state and might better be described as a 1,3-biradical. The ^3B electronic ground state is C_2 symmetric,[9] but with a low barrier to C_{2v} symmetry. An ionisation energy of 8.99 eV was recently determined,[10] in agreement with theory.[11] The electronic spectroscopy and photochemistry of HCCCH have only been investigated in rare gas matrices.[9,12,13] Two broad bands with an unassigned fine structure have been found.[9] The lower one can be assigned to a combination of the 2 ^3B and 1 ^3A states, starting at around 376 nm and maximizing at around 300 nm.[14,15] The more intense second band starts at around 270 nm and maximizes at 245 nm. Several excited states have been computed in this range, but no conclusive assignment was reported.[14,15] The computed oscillator strengths f_e all lie below $f = 10^{-2}$, thus only small signals can be expected in the experiments. As knowledge on the excited electronic states is still limited, a better computational description of the excited states was one of the goals of this work.

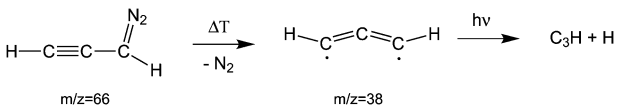

Fig. 1 Propargylene is produced by pyrolysis from diazopropyne. Absorption of a UV-photon leads to H-atom loss and formation of C_3H.

Our main interest is the photodissociation of isolated HCCCH after UV-excitation at around 250 nm. The other two isomers have already been studied by photofragment Doppler-spectroscopy[16,17] and fs time-resolved spectroscopy.[18,19] We apply velocity map imaging (VMI)[20,21] to elucidate the dynamics of propargylene. Only a few reactive intermediates have so far been studied using this method,[22–25] although several radicals have been studied by Rydberg time-of-flight spectroscopy[26,27] or translational energy spectroscopy.[28–31] Four different dissociation channels have been explored by theory:

$$C_3H_2 \rightarrow C_3 + H_2 \quad \Delta_R H(0\ \mathrm{K}) = 259.4\ \mathrm{kJ\ mol^{-1}} \qquad \text{(I)}$$

$$C_3H_2 \rightarrow \text{c-}C_3H + H \quad \Delta_R H(0\ \mathrm{K}) = 374.5\ \mathrm{kJ\ mol^{-1}} \qquad \text{(IIa)}$$

$$C_3H_2 \rightarrow \text{l-}C_3H + H \quad \Delta_R H(0\ \mathrm{K}) = 382.8\ \mathrm{kJ\ mol^{-1}} \qquad \text{(IIb)}$$

$$C_3H_2 \rightarrow C_2H_2 + C\ (^3P) \quad \Delta_R H(0\ \mathrm{K}) = 525.1\ \mathrm{kJ\ mol^{-1}} \qquad \text{(III)}$$

The enthalpies of reaction correspond to the values computed by Mebel *et al.*[14] However, the theoretical values vary over

Institute of Physical and Theoretical Chemistry, University of Würzburg, Am Hubland, D-97074 Würzburg, Germany. E-mail: roland.mitric@uni-wuerzburg.de, ingo.fischer@uni-wuerzburg.de; Tel: +49 931 31-85135, +49 931 31-86360

† Electronic supplementary information (ESI) available: Electronic energies of propargylene computed by CASSCF, molecular orbitals, cuts of the potential energy along the C–H bond distance, reaction rates, a comparison of $P(E_T)$ with a purely statistical model and a Doppler profile recorded at half the excitation laser power. See DOI: 10.1039/c3cp53213e

a considerable range. For channel (IIa) other groups reported values of 379.7 kJ mol^{-1} (ref. 32) and 392.3 kJ mol^{-1} (ref. 33). Loss of H_2 is the lowest energy channel, but is associated with a substantial reverse barrier of 181 kJ mol^{-1}. Channel (III) is spin-forbidden in the photodissociation of cyclopropenylidene and propargylene, but spin-allowed for the photodissociation of triplet propargylene. It becomes accessible only below 228 nm and is therefore ignored further on. We note that within this work we detect hydrogen atoms, *i.e.* we observe channels (IIa) and (IIb), but not channel (I). Note that in the matrix excess energy is transferred to the host and isomerization products can be stabilized. Thus photodissociation was not observed in previous matrix work.

In order to gain a deeper insight into the molecular mechanism underlying the photodissociation process in propargylene under UV irradiation, the experimental investigations are accompanied by a computational study. A theoretical description of photodissociation is still demanding, but in recent years the simulation of coupled electron–nuclear dynamics ''on the fly'' in the framework of Tully's surface hopping method[34] was shown to be a successful approach, as demonstrated *e.g.* for the photodynamics and -fragmentation of several organic and biological molecules,[35–39] where experimentally observed photofragmentation channels could be confirmed. Such computations can be complemented by the simulation of time-resolved spectroscopic observables, as *e.g.* time-resolved photoelectron spectra (*cf. e.g.* ref. 40 and 41), so as to enable the direct comparison with experimental results. Furthermore, this approach has recently been extended to the simulation of angle-resolved quantities, such as time-resolved photoelectron anisotropy maps.[42] However, besides the observation of photoelectrons, angle-resolved measurements can also be used to detect the molecular fragments occurring in dissociation processes. This provides a versatile means to study in more detail the mechanisms of molecular fragmentation and bond breaking. Therefore, in the present contribution, we extend our non-adiabatic surface hopping dynamics ''on the fly'' to the simulation of photofragment angular distributions, which allows us to gain additional insight into the photodissociation dynamics of propargylene.

B Experimental methods

Propargylene was produced from diazopropyne according to Fig. 1 by flash pyrolysis[43] in a jet of helium (3 bar). The precursor was synthesized as reported in the literature,[44] using the modifications described in ref. 10.‡ Diazopropyne decomposes within several hours and has to be freshly prepared before an experiment. In order to suppress the dimerization of propargylene that was already observed in previous experiments,[45] the temperature of the sample container was maintained at 0 °C during the experiment to keep the precursor concentration low.

‡ Diazopropyne is explosive, therefore the preparative protocol has to be accurately followed. The addition of nitroso-propargyl urea described in ref. 44 was carried out under constant argon flow.

The experiments were conducted in a VMI setup,[20,21] described previously.[24] The precursor–seeding gas mixture was expanded through a pulsed solenoid valve at a 10 Hz repetition rate. The carbene was generated in a resistively heated (30–40 W) SiC tube attached to the valve. The skimmed molecular beam entered an ion optics consisting of three plates (repeller, extractor, and ground) 15 mm apart. Fields of 2307 V cm^{-1} and 1056 V cm^{-1} were applied to the electrodes to extract the ions and accelerate them onto the dual stage microchannel plate (MCP) detector equipped with a phosphorescent screen (P43). The voltage at the back plate of the detector was gated by a push–pull switch to detect only hydrogen ions. The resulting ion signal was imaged onto a progressive-scan camera with a 2/3″ CCD chip by an achromatic lens. The H-atom images were accumulated over 10 000 laser shots, symmetrized and reconstructed with the pBASEX algorithm,[46] using Legendre polynomials up to 2nd order.

For excitation the unfocused frequency-doubled output of a Nd:YAG laser pumped dye laser (around 2 mJ) was used. The H-atom photofragments were ionized by [1+1′] multiphoton ionization (MPI). To produce tunable VUV radiation at around 121.6 nm (Lyman-α) that excites the $^2S \rightarrow {}^2P$ transition of H, the output of a second frequency-doubled dye laser was focused into a cell filled with 90 Torr of Kr. A 100 mm MgF_2 lens mounted at the exit of the cell focusses the VUV light into the ionization region. The remaining fundamental ionises the excited H-atoms. To cover the whole Doppler profile of the H-atoms, the laser was scanned over ± 6 cm^{-1} around the Lyman-α transition. In most of the experiments described below the ionization laser was delayed by 10–30 ns with respect to the excitation laser. The two laser systems were synchronized electronically to within 1 ns and polarized perpendicularly with respect to each other by a Fresnel double rhomb. To minimize contributions from one-colour processes a background image was recorded without the excitation laser and subtracted from the two-colour image. The current at the back plate of the microchannel plate ion detector was monitored to record the time of flight (TOF) mass spectra. The TOF mass spectra were recorded at an ionization wavelength of 118 nm for better detection efficiency. In these experiments the gas cell for tripling (*vide supra*) was filled with Xe.

C Computational methods

The electronic absorption spectrum of propargylene was described using the multireference configuration interaction (MRCI) method[47–49] as implemented in the MOLPRO program package.[50] This involves the generation of all single and double excitations out of a set of reference wavefunctions, which have been obtained using the state-averaged complete active space self-consistent field (CASSCF) method[51,52] employing the atomic natural orbital triple zeta (ANO-TZ) basis set of Roos *et al.*[53] The active space comprised 6 electrons in 7 orbitals. Overall, seven electronic states were included in the MRCI and CASSCF calculations, and the electronic state energies were determined employing the Davidson-type correction[54] Q2 of Werner *et al.*[55] which approximately accounts for the effect of disconnected quadruple excitations.

Temperature broadening of the absorption spectrum has been simulated by sampling 100 nuclear geometries from a canonical Wigner distribution function of the harmonic normal modes of the system at 100 K.[56] To obtain the latter, a computationally more efficient approach has been used, employing the state-averaged CASSCF method and an uncontracted version of the smaller polarized valence double zeta (pVDZ) basis set of Ahlrichs *et al.*,[57,58] which has been augmented by diffuse basis functions from the aug-cc-pVDZ basis set of Dunning *et al.*[59] in order to properly describe spatially extended Rydberg-like molecular orbitals of the system. Specifically, a single diffuse *s* function for hydrogen atoms, as well as one *s* and three cartesian *p* functions for carbon were added.

The photodynamics of propargylene in the ground and six excited electronic triplet states has been simulated using Tully's surface hopping method[34] combined with the state-averaged CASSCF procedure and the above-mentioned uncontracted pVDZ basis set augmented by diffuse functions. In addition, the active space was extended to 8 electrons in 8 orbitals in order to qualitatively correctly describe the C–H fragmentation frequently taking place during the dynamics. A number of 100 initial coordinates and momenta were generated from the canonical Wigner distribution of the system's vibrational normal modes at 100 K (*cf.* above). The nuclear trajectories were propagated by integrating the classical Newtonian equations of motion using the velocity Verlet algorithm.[60,61] For this purpose, a time step of 0.2 fs was employed, and the forces acting on the nuclei were obtained by numerical differentiation of the electronic energies using the central difference approximation.

Initially, all trajectories were started in the sixth excited state T_6 corresponding to the most intense electronic transition (see below). Subsequently, in order to determine the electronic state during the dynamics, the electronic Schrödinger equation

$$i\hbar\dot{c}_i[t,\mathbf{R}(t)] = E_i[\mathbf{R}(t)]c_i[t,\mathbf{R}(t)] - i\hbar\sum_j D_{ij}[\mathbf{R}(t)]c_j[t,\mathbf{R}(t)] \quad (1)$$

was integrated numerically along each trajectory $\mathbf{R}(t)$ using the fourth order Runge Kutta procedure with a time step of 8×10^{-5} fs. The scalar nonadiabatic coupling was obtained as $D_{ij} = \dot{\mathbf{R}}\cdot\mathbf{d}_{ij}$ by numerically calculating the component of the nonadiabatic coupling vector $\mathbf{d}_{ij} = \langle\Psi_i|\nabla_{\mathbf{R}}|\Psi_j\rangle$ in the direction of the nuclear velocities $\dot{\mathbf{R}}$. To this end, the derivative with respect to the nuclear displacement along $\dot{\mathbf{R}}$ was approximated by finite differences, as implemented in the *DDR* routine of the MOLPRO package.[50] During the dynamics, the couplings between the actual state and the next-neighbouring upper and lower states were taken into account.

The time-dependent electronic state populations $\rho_{ii} = |c_i|^2$ obtained in this way were subsequently employed to calculate hopping probabilities in the framework of the surface hopping procedure according to ref. 62 as

$$P_{i\to j} = \Theta(-\dot{\rho}_{ii})\Theta\left(\dot{\rho}_{jj}\right)\frac{-\dot{\rho}_{ii}}{\rho_{ii}}\frac{\dot{\rho}_{jj}}{\sum_k \Theta(\dot{\rho}_{kk})\dot{\rho}_{kk}}\Delta t \quad (2)$$

where Δt is the nuclear time step, and the Θ functions are defined to be unity for positive arguments and zero otherwise.

The individual trajectories were propagated over a time duration of 200 fs at maximum, alternatively terminating after completion of the C–H fragmentation. The kinetic energy distribution of the H atoms released in this process was obtained from the subset of all fragmenting trajectories of the ensemble. For the angle-resolved distribution, the anisotropy parameter β_2 can be calculated according to ref. 63 in molecular frame coordinates from the distribution $\mathscr{P}(\theta)$ of the angle θ between the initial transition dipole moment for the $T_0 \rightarrow T_6$ excitation and the momentum vector of the released H atoms as

$$\beta_2 = \int_0^\pi P_2(\cos\theta)\mathscr{P}(\theta)\mathrm{d}\theta \quad (3)$$

where P_2 is the second Legendre polynomial. In the case of individual trajectories, the distribution $\mathscr{P}(\theta)$ reduces to a sum over delta functions,

$$\mathscr{P}(\theta) = \frac{1}{N_{\mathrm{traj}}}\sum_n \delta(\theta-\theta_n) \quad (4)$$

leading to

$$\beta_2 = \frac{1}{N_{\mathrm{traj}}}\sum_n P_2(\cos\theta_n) = \frac{1}{2N_{\mathrm{traj}}}\sum_n \left(3\cos^2\theta_n - 1\right). \quad (5)$$

The angle-resolved intensity in the lab frame has been subsequently obtained according to

$$I(\theta_{\mathrm{L}}) = \frac{1}{4\pi}[1 + \beta_2 P_2(\cos\theta_{\mathrm{L}})] \quad (6)$$

where θ_{L} denotes the angle of fragment recoil in the lab frame coordinate system.[63]

D Results and discussion

Fig. 2 shows typical mass spectra. Without pyrolysis and only the 118 nm ionization laser present (Fig. 2a, top trace), the precursor, diazopropyne (m/z = 66), as well as propargylene (m/z = 38) generated by dissociative photoionization are visible. The appearance energy $AE_{0K}(C_3H_2N_2, C_3H_2^+)$ has been determined to be 9.25 eV.[10] When the pyrolysis is turned on, the diazopropyne peak disappears and only a peak at m/z = 38 due to propargylene is visible. We employed 118 nm radiation for photoionisation mass spectrometry due to its higher efficiency. Using 121.6 nm all mass peaks except that for hydrogen were barely above the noise level, because a diluted sample was used to suppress dimerization (*vide supra*).

Experiments were conducted at 250 nm (4.96 eV), close to the maximum of the second absorption band. As knowledge on the initially excited state is necessary for an appropriate characterisation of the subsequent dynamics, the absorption spectrum of propargylene was computed in the framework of CAS-MRCI as detailed in the Computational section. The theoretical temperature-broadened (100 K) electronic absorption spectrum of propargylene is shown in Fig. 3 (upper panel). The spectrum

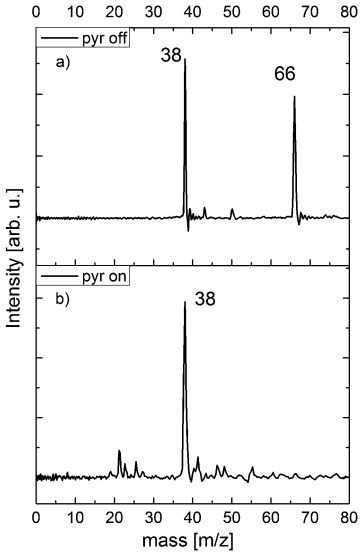

Fig. 2 Photoionization mass spectra using 118 nm radiation show an almost complete conversion of the precursor in the pyrolysis (lower trace). Without pyrolysis (upper trace) a significant amount of $C_3H_2^+$ is present due to dissociative photoionization.

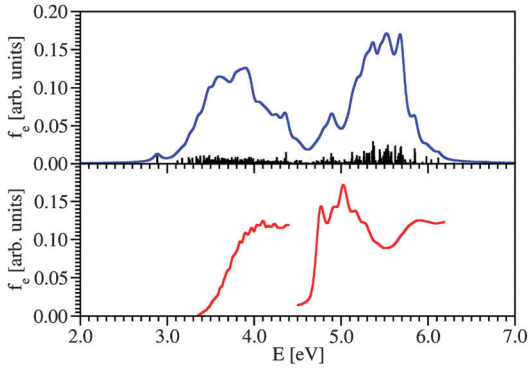

Fig. 3 Upper panel: simulated temperature-broadened electronic absorption spectrum of propargylene obtained by the CAS-MRCI method employing the Davidson correction in a rotated reference space.[54] Lower panel: experimental UV/vis absorption spectrum of Seburg *et al.*[9] The heights of the two experimental bands have been scaled independently since due to the presence of the strongly absorbing precursor diazopropyne, the absorption intensities at different wavelengths are not comparable (*cf.* suppl. information of ref. 9).

is characterized by two absorption bands centred at around 3.8 eV and 5.5 eV. For comparison, the UV/Vis spectrum recorded by Seburg *et al.*[9] is shown in the lower panel of the figure. Both spectra agree qualitatively, although the bands are somewhat shifted with respect to each other, the experimental peaks being situated at around 4.0 and 5.0 eV. Note that the temperature of 100 K in the computations was chosen for a comparison with the gas-phase experiments. In contrast the Ar-matrix in the experiments of Seburg *et al.* was at around 8 K.[9]

The figure also shows that the structure of the spectrum originates from several overlapping electronic transitions and is not due only to vibrational progressions of a single transition.

Table 1 Excited electronic states of propargylene obtained using CAS-MRCI (6 electrons in 7 orbitals, ANO-TZ basis)

State[a]	E (MR-CISD)/ eV	E (MR-CISD + Q)[b]/eV	Dominant configuration[c]	Character	f_e
T_0 (^{3}B)	0.00	0.00	2 2//0 0 0 (86%)	Ground state	—
T_1 (1^3A)	3.68	3.65	/ 2 2/0 0 0 (60%)	ππ*	0.0035
T_2 (2^3B)	3.85	3.82	2/2/0 0 0 (78%)	ππ*	0.0002
T_3 (2^3A)	4.09	4.05	2//2 0 0 0 (69%)	ππ*	0.0023
T_4 (3^3B)	4.33	4.29	/ 2/2 0 0 0 (78%)	ππ*	0.0001
T_5 (4^3B)	5.19	4.96	2 2/0/0 0 (58%) 2 2/0 0/0 (19%)	Rydberg s ππ*	0.0003
T_6 (3^3A)	5.90	5.49	2 2 0//0 0 (48%) 2 2/0 0 0/ (22%)	Rydberg s ππ*	0.0166

[a] Approximate symmetry labelling according to the C_2 point group. The molecular structure has been optimized without symmetry restrictions and therefore deviates marginally from exact C_2 symmetry. [b] Davidson correction in rotated reference space, *cf.* Method Q2 in ref. 55. [c] Only configurations having a weight of more than 10% are tabulated. The occupation of the active orbitals is given as: 2 – doubly occupied, / – singly occupied, 0 – unoccupied.

The character of the excited electronic states contributing to the absorption spectrum is summarized in Table 1, together with the vertical excitation energies calculated at the ground state equilibrium geometry and the oscillator strength f_e for the corresponding transitions. The data show that the low-energy absorption is mainly due to the presence of ππ* electronic states, whereas the absorption above 4.8 eV largely originates from excited states bearing s Rydberg character. The character of the molecular orbitals can be identified from their spatial shape as shown in Fig. S1 of the ESI.† The computations confirm that the oscillator strengths are small as reported previously. The T_6 state has the by far highest oscillator strength and contributes to the largest part of the intensity of the second absorption peak (*cf.* Table 1). Therefore we assume that excitation at 250 nm predominately populates this state, although the CAS-MRCI excitation energy is almost 0.5 eV higher.

An experimental challenge of the present study lies in the photochemistry of the precursor. Diazopropyne absorbs at least in the matrix in the same wavelength region as propargylene, but the cross section is considerably larger.[9] In our experiments it is found to also lose H-atoms upon photoexcitation at around 250 nm. Therefore complete conversion as seen in Fig. 2b is mandatory to study photodissociation dynamics of propargylene. To understand the possible background contribution from the precursor, we investigated the H-atom loss from diazopropyne in a first series of experiments at 250 nm (4.96 eV) and found a dependence on the excitation laser power that is greater than linear. The resulting translational energy distribution $P(E_T)$ is given as a dashed line in Fig. 4.

In a next step H-atom images were recorded with active pyrolysis in order to study the photodissociation dynamics of propargylene.

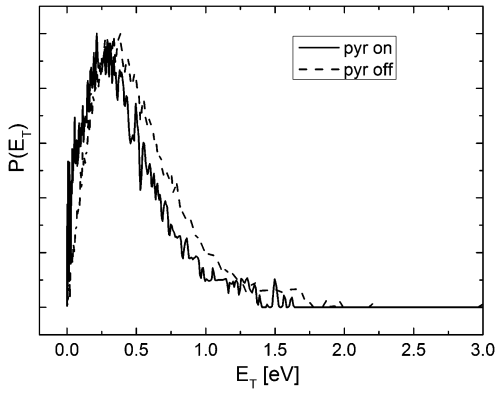

Fig. 4 Translational energy distribution $P(E_T)$ with pyrolysis on (solid line) and off (dashed line). As visible the distribution is shifted to *lower* energies with pyrolysis.

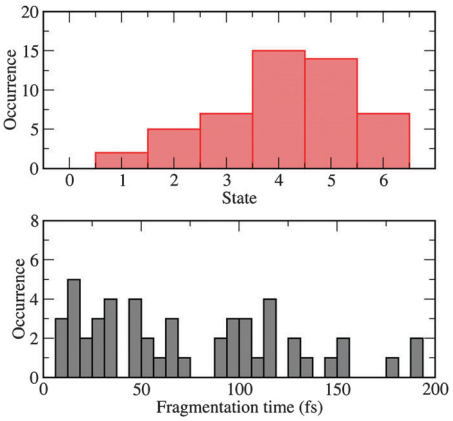

Fig. 5 Upper panel: distribution of electronic states in which the C–H dissociation takes place. Lower panel: distribution of the time instants when the dissociation occurs during the dynamics.

The $P(E_T)$ derived from this image is given as a solid line in Fig. 4. As visible the shape of the distribution is very similar, but with pyrolysis the maximum is shifted by around 0.1 eV to *lower* kinetic energies. Note that a simple heating effect in the pyrolysis would lead to H-atoms with a *higher* kinetic energy.

We interpret these observations as follows: absorption of a first photon in the precursor leads to photodissociation to C_3H_2 + N_2. In fact irradiation at 254 nm[13] and 472 nm[12] has been used to generate HCCCH in rare gas matrices. The propargylene fragment can then absorb a second UV-photon and loses a hydrogen atom in a second dissociation step. In both cases, with and without pyrolysis, H-atoms are formed from propargylene, so a similar $P(E_T)$ can be expected. However, HCCCH produced by pyrolysis is cooled in the subsequent expansion and possesses less internal excitation.

As noted above we assume that the absorption at around 5 eV is dominated by a transition to the T_6 state, which contributes the largest part of the intensity of the second absorption peak (*cf.* Table 1). Therefore the simulation of the photodynamics of propargylene was started in this state. Due to its higher computational efficiency, the CASSCF method employing a smaller pVDZ basis set was used for the dynamics simulation. This implicates that part of the dynamical electron correlation is neglected and leads to considerable shifts of the excitation energies (*cf.* ESI,† Table S1). It nevertheless allows for a qualitatively correct description of the electronic structure, as can be inferred from the very similar characters of the electronic states as compared to the MRCI case (*cf.* also Table S1, ESI†).

A total of 100 classical surface-hopping trajectories were propagated for 200 fs at maximum, terminating earlier when C–H bond dissociation took place. Overall, the latter occurs in 50% of the trajectories and mainly proceeds in the higher excited states T_4–T_6, as shown in Fig. 5 (upper panel). Non-dissociative trajectories mainly remain in the manifold of the T_5 and T_6 states throughout the dynamics, with only a minor part undergoing internal conversion to lower excited states. No dissociation in the electronic ground state was observed within the first 200 fs, which strongly hints at a mechanism that is linked with the specific shape of the potential energy surfaces of several higher excited states. Cuts of the potential energy along the C–H bond distance seem to confirm a predissociative mechanism. These cuts are given in the ESI,† Fig. S2. For most of the trajectories, dissociation occurred within a propagation time of less than 100 fs, while a minor part only dissociated within 200 fs (*cf.* lower part of Fig. 5). This is also evident from the time-dependent C–H bond distances depicted in Fig. 6. The superposition of the initial and final structures for the dissociative trajectories in the lower panel shows a significant rearrangement of the molecular structure during photodissociation. Many vibrational degrees of freedom get excited during the nonradiative deactivation, and redistribution of vibrational energy is fast.

Experimentally we investigated the rate of H-atom formation by delaying the two lasers with respect to each other, but the rise time of the H-atom signal was faster than the time resolution of our setup ($\approx$10 ns), see Fig. S3 (ESI†). This is in full

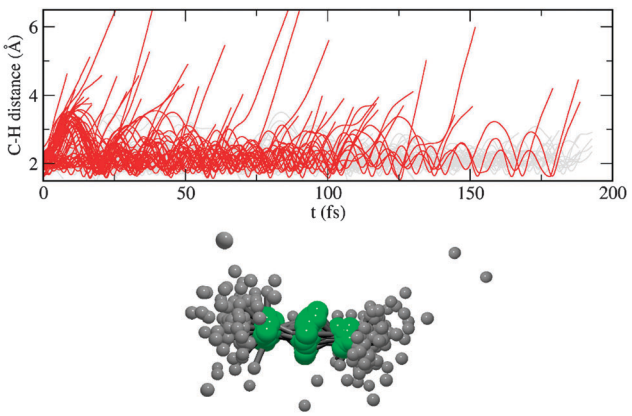

Fig. 6 Upper panel: time-dependent C–H bond distances for the ensemble of trajectories. The distance between each H atom and the initially nearest-neighbouring C atom is shown. Dissociating bonds are represented by red curves, the remaining part by grey ones. Lower panel: superposition of the initial and final structures of propargylene for the dissociating trajectories. The green balls represent the carbon atoms, the grey ones the hydrogen atoms.

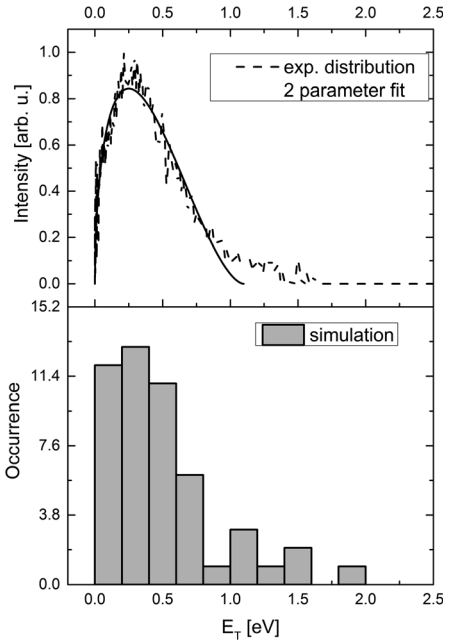

Fig. 7 Upper trace: translational energy distribution of H-atoms from propargylene (dashed line), fitted with a two-parameter function (solid line). Lower trace: kinetic energy distribution of the dissociated H atoms, shown as a histogram of 50 dissociating trajectories.

agreement with the femtosecond dissociation times found in the calculations.

The translational energy distribution of the H-atom photofragments $P(E_T)$ is the main experimental observable and has to be described properly by a valid theoretical model. The distribution for the H-atoms generated from propargylene is again depicted in Fig. 7. It peaks at 0.25 eV, which corresponds to 24 kJ mol^{-1}. No fine structure due to excitation of product vibrations is visible, because the vibrational energy is rapidly distributed before photodissociation, as can be concluded from the structures of propargylene for the dissociating trajectories depicted in the lower trace of Fig. 6. To obtain an expectation value for the translational energy release it was fitted using the following function:[64]

$$P(f_T) = C f_T^a (1 - f_T)^b \quad (7)$$

In this equation f_T represents the fraction of the total available translational energy, the exponents a and b are fit parameters and C is a normalization constant, chosen to scale the fit to the experimental data. The values of a and b were iteratively optimized until a least-square fit had converged. Note that expression (7) is empirical and does not assume any dissociation mechanism. The best fit is given in Fig. 7 as a solid line. It is based on the maximum excess energy of 1.1 eV (104 kJ mol^{-1}) assuming channel (IIa), but experimentally we cannot distinguish between channels (IIa) and (IIb). As visible the fit is quite good, but a fraction of H-atoms shows a translational energy higher than the available maximum. Possible reasons will be discussed below. The expectation value $\langle E_T \rangle$ of the H-atoms is derived from eqn (2) to be $\langle E_T \rangle$ = 0.53 eV, which corresponds to $\langle f_T \rangle$ = 0.48. This value is clearly above the limit expected for a statistical dissociation process. Typical values for $\langle f_T \rangle$ observed in the photodissociation of aromatic molecules are around 0.1. In recent experiments on reactive species we measured $\langle f_T \rangle$ = 0.09 for fulvenallene[65] and $\langle f_T \rangle$ = 0.19 for ethyl.[24] In Fig. S4 (ESI†) the experimental distribution is compared with the computed distribution expected for an ideal statistical reaction. As visible such a statistical distribution does not match the experimental one. Therefore a statistical dissociation on the ground state potential energy surface can be ruled out from the experiment.

The lower trace of Fig. 7 depicts computational results for comparison. The *y*-axis represents the number of trajectories that yield translational energies within a 0.2 eV interval (width of the columns). The hydrogen atoms released during the dissociation process bear translational energies mainly below 1 eV, with the energy distribution centered at about 0.3 eV, very close to the maximum of the experimental distribution. It is evident from Fig. 7 that the computed $P(E_T)$ agrees well with the experimental one. It should be noted that 50% of the trajectories do not dissociate within the propagation time. A part of them might deactivate to the electronic ground state and dissociate there on a much longer time scale, *i.e.* in a statistical fashion, which could modify the translational energy distribution.

We also analysed the photofragment angular distribution (PAD) of the H-atoms, as depicted in Fig. 7. The centre trace shows the experimental PAD of the H-atoms with pyrolysis. The data were fitted using the standard recoil anisotropy function given in eqn (6), with the anisotropy parameter β being optimized in the fit. The PAD of the H-atoms generated by the photodissociation of propargylene is almost isotropic with a small β-parameter of -0.05. This is unusual for an excited-state dissociation that is faster than molecular rotation, which generally leads to large β-values.

Interestingly the angular distribution of the H-atoms without pyrolysis is somewhat different. The distribution of the H-atom photofragments generated *via* photodissociation of the precursor is anisotropic with a β-parameter of -0.19 (top trace). Two effects contribute to the larger anisotropy. First, the photodissociation of diazopropyne yields a prealigned sample of propargylene molecules, so an additional transition dipole moment vector has to be considered. Second, the propargylene formed by photodissociation of the precursor gains some of the excess energy E_{excess} as an additional internal energy, thus the $P(E_T)$ of the H-atom products will be shifted to higher kinetic energies, as observed. Dissociation might be accelerated by the higher internal energy, leading to a higher degree of anisotropy.

In the frame of our nonadiabatic dynamics simulations, also the anisotropy parameter for the H atom distribution can be straightforwardly computed. As outlined in the computational section, the necessary ingredients are the vectorial velocities of the released H atoms as well as the transition dipole moments for the initial excitation, which are illustrated schematically in Fig. 9. The angle between these two quantities is utilized according to eqn (6) in order to yield the β parameter, which in the present simulation assumes a value of -0.03. This allows

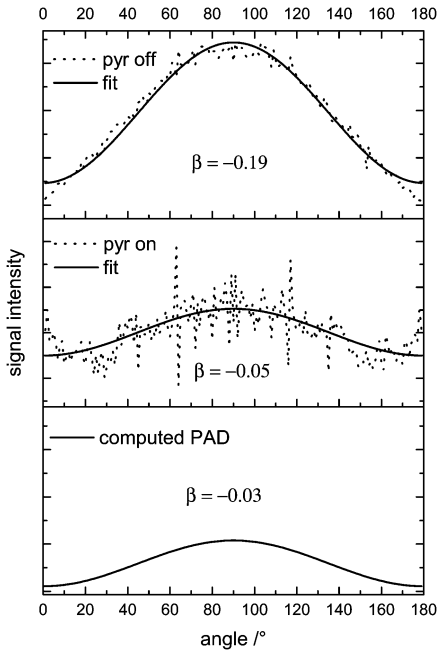

Fig. 8 H-atom photofragment angular distribution with pyrolysis off (top trace) and on (centre trace). The computed PAD is given for comparison in the bottom trace.

for the calculation of the angle-resolved intensity in the laboratory frame coordinates shown in Fig. 8. As visible the experimental PAD is very well represented by the computed one. Fig. 9 indicates that the small anisotropy is due to the fact that the photofragments are emitted over a range of angles that is not too far from the magic angle.

As discussed above a small signal is visible at the $P(E_T)$ above 1.1 eV. It might be due to (a) multiphoton excitation, (b) a $\Delta_R H$ that is slightly smaller than computed, (c) photodissociation of propargylene molecules photolytically formed from a residual precursor, or (d) vibrationally excited propargylene molecules

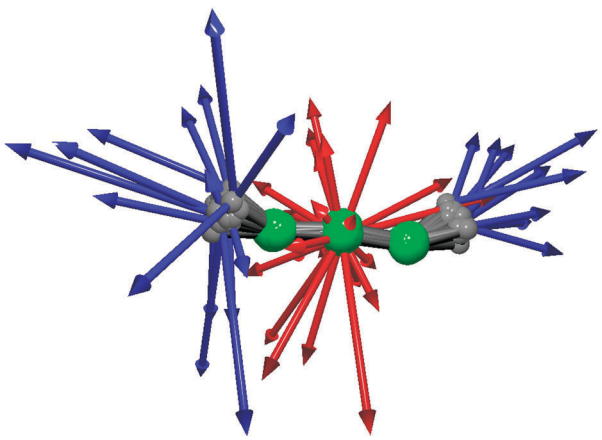

Fig. 9 Illustration of absolute values and directions of the H atom velocities upon dissociation (blue arrows) together with the initial transition dipole moments for the T_0–T_6 excitation (red arrows). The blue arrows have been scaled by a factor of 50, the red ones by 0.5.

that acquired some internal energy in the pyrolysis. The H-atom signal depends linearly on the laser power, so a large contribution from higher order processes is unlikely. Doppler profiles were recorded at different excitation powers, but showed no significant difference in $\langle E_T \rangle$ (see Fig. S5 of ESI†). The reaction enthalpy, computed by coupled cluster theory, CCSD(T),[14] could be off by a few kJ mol^{-1}, which might partly explain the signal. On the other hand, since the absorption cross section of the precursor at 250 nm is considerably larger than that of HCCCH, even small amounts of precursor that are not observed in the mass spectrum are able to produce a detectable signal. In fact the β-value of the fastest H-atoms seems to be more negative ($\beta \approx -0.16$), indicating some contribution from the unconverted precursor. Nevertheless we also consider vibrationally excited carbenes, (d) to contribute significantly to the signal above 1.1 eV. This is also confirmed by the computations that show a few trajectories with a high kinetic energy release, because thermal energy present before photoexcitation is also liberated as translation. Their number depends on the internal temperature of the sample, which is 100 K in the present simulations. Such temperatures are quite typical for pyrolytically generated radicals in a free jet. For allyl for example a rotational temperature of 150 K was determined.[66] Given the agreement with the experiment, this seems to be a realistic assumption for the temperature of jet-cooled HCCCH.

We also studied propargylene upon excitation between 315 nm and 325 nm, *i.e.* around the dissociation threshold of 319.4 nm. In this wavelength region the absorption cross section σ_{abs} of HCCCH is smaller than that at 250 nm, but larger than σ_{abs} of the precursor. A small H-atom signal was observed, but the signal/noise ratio was too low for a conclusive analysis. Presumably channel (I) dominates at energies close to the barrier.

E Summary and conclusion

The photodissociation of propargylene, HCCCH, at 250 nm has been studied experimentally by velocity map imaging of H-atom photofragments and theoretically by nonadiabatic surface hopping calculations. The observed H-atom translational energy distribution maximises at 0.25 eV, while the simulations showed a high probability for a translational energy release between 0.2 and 0.4 eV. Also the photofragment angular distribution is well represented. The experimental β-parameter of -0.05 has to be compared with a computed one of $\beta = -0.03$. Thus the computations cover the essential characteristics of the photodissociation process and describe the main features properly. The computations indicate that propargylene is photoexcited to the T_6 state, which carries the by far highest oscillator strength in the energy region of interest. The trajectory calculations show a rapid nonradiative deactivation of the initially excited state and a photodissociation that occurs predominately in the T_4–T_6 excited states. However, roughly 50% of the trajectories do not dissociate within the 200 fs propagation time, thus an additional contribution of dissociation in the electronic ground state is possible.

Several experimental challenges have to be addressed. First of all a full conversion of the precursor diazopropyne is mandatory,

because it has a high absorption cross section at 250 nm and also loses H-atoms. It was shown that the H-loss occurred also from propargylene, formed photolytically from the precursor. Photolytically produced HCCCH has more internal energy, because it is not cooled in the expansion. As a consequence the translational energy distribution is shifted to higher energies. A more pronounced anisotropy in the photofragment angular distribution is also present. The second challenge is propargylene's tendency to dimerise. Therefore the sample was cooled and the precursor diluted. Dimerisation was successfully suppressed, but in combination with the low oscillator strengths this leads to small photofragment signals from propargylene.

Acknowledgements

Financial support from the Deutsche Forschungsgemeinschaft through contract FI575/8-2 is gratefully acknowledged. JG thanks the *Fonds der Chemischen Industrie* (FCI) for a fellowship. We would like to thank Melanie Lang and Engelbert Reusch for their assistance in the experiment.

Notes and references

1 P. Thaddeus, C. A. Gottlieb, R. Mollaaghababa and J. M. Vrtilek, *J. Chem. Soc., Faraday Trans.*, 1993, **89**, 2125.
2 H. Liszt, P. Sonnentrucker, M. Cordiner and M. Gerin, *ApJ*, 2012, **753**, L28.
3 J. M. Vrtilek, C. A. Gottlieb and P. Thaddeus, *ApJ*, 1987, **314**, 716.
4 J. A. Hodges, R. J. McMahon, K. W. Sattelmeyer and J. F. Stanton, *ApJ*, 2000, **544**, 838.
5 J. P. Maier, G. A. H. Walker, D. A. Bohlender, F. J. Mazzotti, R. Raghunandan, J. Fulara, I. Garkusha and A. Nagy, *ApJ*, 2011, **726**, 41.
6 C. A. Taatjes, S. J. Klippenstein, N. Hansen, J. A. Miller, T. A. Cool, J.-K. Wang, M. E. Law and P. R. Westmoreland, *Phys. Chem. Chem. Phys.*, 2005, **7**, 806.
7 J. F. Stanton, *Faraday Discuss.*, 2011, **150**, 331.
8 J. F. Stanton, E. Garand, J. Kim, T. I. Yacovitch, C. Hock, A. S. Case, E. M. Miller, Y.-J. Lu, K. M. Vogelhuber, S. W. Wren, T. Ichino, J. P. Maier, R. J. McMahon, D. L. Osborn, D. M. Neumark and W. C. Lineberger, *J. Chem. Phys.*, 2012, **136**, 134312.
9 R. A. Seburg, E. V. Patterson and R. J. McMahon, *J. Am. Chem. Soc.*, 2009, **131**, 9442.
10 M. Steinbauer, M. Lang, I. Fischer, B. K. Cunha de Miranda, C. Romanzin and C. Alcaraz, *Phys. Chem. Chem. Phys.*, 2011, **13**, 17956.
11 K. C. Lau and C. Y. Ng, *Chin. J. Chem. Phys.*, 2006, **19**, 29.
12 R. A. Seburg and R. J. McMahon, *Angew. Chem., Int. Ed. Engl.*, 1995, **34**, 2009.
13 R. A. Seburg, E. V. Patterson, J. F. Stanton and R. J. McMahon, *J. Am. Chem. Soc.*, 1997, **119**, 5847.
14 A. M. Mebel, W. M. Jackson, A. H. H. Chang and S. H. Lin, *J. Am. Chem. Soc.*, 1998, **120**, 5751.
15 M. C. van Hemert and E. F. van Dishoeck, *Chem. Phys.*, 2008, **343**, 292.
16 C. Groß, B. Noller and I. Fischer, *Phys. Chem. Chem. Phys.*, 2008, **10**, 5196.
17 P. Hemberger, B. Noller, M. Steinbauer, K. Fischer and I. Fischer, *J. Phys. Chem. Lett.*, 2010, **1**, 228.
18 B. Noller, M. Margraf, C. Schröter, T. Schultz and I. Fischer, *Phys. Chem. Chem. Phys.*, 2009, **11**, 5353.
19 P. Hemberger, J. Koehler, I. Fischer, G. Piani, L. Poisson and J.-M. Mestdagh, *Phys. Chem. Chem. Phys.*, 2012, **14**, 6173.
20 *Imaging in Molecular Dynamics*, ed. B. J. Whitaker, Cambridge University Press, Cambridge, 2003.
21 A. T. J. B. Eppink and D. H. Parker, *Rev. Sci. Instrum.*, 1997, **68**, 3477.
22 M. Ryazanov, C. Rodrigo and H. Reisler, *J. Chem. Phys.*, 2012, **136**, 084305.
23 B. W. Alligood, C. C. Womack, D. B. Straus, F. R. Blase and L. J. Butler, *J. Chem. Phys.*, 2011, **134**, 194304.
24 M. Steinbauer, J. Giegerich, K. H. Fischer and I. Fischer, *J. Chem. Phys.*, 2012, **137**, 014303.
25 C. Rodrigo, C. Zhou and H. Reisler, *J. Phys. Chem. A*, 2013, **117**, 12049.
26 G. Amaral, K. Xu and J. Zhang, *J. Chem. Phys.*, 2001, **114**, 5164.
27 S. H. S. Wilson, J. D. Howe, K. N. Rosser, M. N. R. Ashfold and R. N. Dixon, *Chem. Phys.*, 1994, **227**, 456.
28 L. J. Butler and D. M. Neumark, *J. Phys. Chem.*, 1996, **100**, 12801.
29 B. Negru, S. J. Goncher, A. L. Brunsvold, G. M. P. Just, D. Park and D. M. Neumark, *J. Chem. Phys.*, 2010, **133**, 074302.
30 B. Negru, G. M. P. Just, D. Park and D. M. Neumark, *Phys. Chem. Chem. Phys.*, 2011, **13**, 8180.
31 J. D. Savee, J. E. Mann, C. M. Laperle and R. E. Continetti, *Int. Rev. Phys. Chem.*, 2011, **30**, 79.
32 C. Ochsenfeld, R. I. Kaiser, Y. T. Lee, A. G. Suits and M. Head-Gordon, *J. Chem. Phys.*, 1997, **106**, 4141.
33 A. Mohajeri and M. J. Jenabi, *THEOCHEM*, 2007, **820**, 65.
34 J. C. Tully, *J. Chem. Phys.*, 1990, **93**, 1061.
35 E. Martínez-Núñez, S. Vázquez, G. Granucci, M. Persico and C. M. Estevez, *Chem. Phys. Lett.*, 2005, **412**, 35.
36 I. Antol, M. Eckert-Maksić, M. Barbatti and H. Lischka, *J. Chem. Phys.*, 2007, **127**, 234303.
37 M. D. Lodriguito, G. Lendvay and G. C. Schatz, *J. Chem. Phys.*, 2009, **131**, 224320.
38 M. Wohlgemuth, V. Bonačić-Koutecký and R. Mitrić, *J. Chem. Phys.*, 2011, **135**, 054105.
39 G. Tomasello, M. Wohlgemuth, J. Petersen and R. Mitrić, *J. Phys. Chem. B*, 2012, **116**, 8762.
40 R. Mitrić, U. Werner and V. Bonačić-Koutecký, *J. Chem. Phys.*, 2008, **129**, 164118.
41 R. Mitrić, J. Petersen, M. Wohlgemuth, U. Werner, V. Bonačić-Koutecký, L. Wöste and J. Jortner, *J. Phys. Chem. A*, 2011, **115**, 3755.
42 A. Humeniuk, M. Wohlgemuth, T. Suzuki and R. Mitrić, *J. Chem. Phys.*, 2013, **139**, 134104.
43 D. W. Kohn, H. Clauberg and P. Chen, *Rev. Sci. Instrum.*, 1992, **63**, 4003.

44 G. Maier, H.-P. Reisenauer, W. Schwab, P. Carsky, V. Spirko, B. A. Hess Jr. and L. J. Schaad, *J. Chem. Phys.*, 1989, **91**, 4763.
45 H. Clauberg, D. W. Minsek and P. Chen, *J. Am. Chem. Soc.*, 1992, **114**, 99.
46 G. Garcia, L. Nahon and I. Powis, *Rev. Sci. Instrum.*, 2004, **75**, 4989.
47 P. J. Knowles and H. J. Werner, *Chem. Phys. Lett.*, 1988, **145**, 514.
48 P. J. Knowles and H. J. Werner, *Theor. Chim. Acta*, 1992, **84**, 95.
49 H. J. Werner and P. J. Knowles, *J. Chem. Phys.*, 1988, **89**, 5803.
50 H.-J. Werner, P. J. Knowles, G. Knizia, F. R. Manby, M. Schütz *et al.*, Molpro, version 2010.1, a package of ab initio programs, see http://www.molpro.net.
51 P. J. Knowles and H. J. Werner, *Chem. Phys. Lett.*, 1985, **115**, 259.
52 H. J. Werner and P. J. Knowles, *J. Chem. Phys.*, 1985, **82**, 5053.
53 P.-O. Widmark, P.-A. Malmqvist and B. O. Roos, *Theor. Chim. Acta*, 1990, **77**, 291.
54 E. R. Davidson and D. W. Silver, *Chem. Phys. Lett.*, 1977, **52**, 403.
55 H.-J. Werner, M. Kallay and J. Gauss, *J. Chem. Phys.*, 2008, **128**, 034305.
56 M. Hillery, R. F. Oconnell, M. O. Scully and E. P. Wigner, *Phys. Rep.*, 1984, **106**, 121.
57 A. Schäfer, H. Horn and R. Ahlrichs, *J. Chem. Phys.*, 1992, **97**, 2571.
58 K. L. Schuchardt, B. T. Didier, T. Elsethagen, L. Sun, V. Gurumoorthi, J. Chase, J. Li and T. L. Windus, *J. Chem. Inf. Model.*, 2007, **47**, 1045.
59 R. A. Kendall, T. H. Dunning Jr. and R. J. Harrison, *J. Chem. Phys.*, 1992, **96**, 6796.
60 L. Verlet, *Phys. Rev.*, 1967, **159**, 98.
61 W. C. Swope, H. C. Andersen, P. H. Berens and K. R. Wilson, *J. Chem. Phys.*, 1982, **76**, 637.
62 R. Mitrić, J. Petersen and V. Bonačić-Koutecký, in *Advanced Series in Physical Chemistry*, ed. W. Domcke, D. R. Yarkony and H. Köppel, World Scientific, Singapore, 2011, vol. 17 Conical Intersections – Theory, Computation and Experiment.
63 G. E. Busch and K. R. Wilson, *J. Chem. Phys.*, 1972, **56**, 3638.
64 S. W. North, A. J. Marr, A. Furlan and G. E. Hall, *J. Phys. Chem. A*, 1997, **101**, 9224.
65 J. Giegerich and I. Fischer, *Phys. Chem. Chem. Phys.*, 2013, **15**, 13162.
66 D. W. Minsek, J. A. Blush and P. Chen, *J. Phys. Chem.*, 1992, **96**, 2025.

